

Micrometer-Scale Deep-Level Spectral Photoluminescence From Dislocations in Multicrystalline Silicon

Hieu T. Nguyen, Fiacre E. Rougieux, Fan Wang, Hoe Tan, and Daniel Macdonald

Abstract—Micrometer-scale deep-level spectral photoluminescence (PL) from dislocations is investigated around the subgrain boundaries in multicrystalline silicon. The spatial distribution of the D lines is found to be asymmetrically distributed across the subgrain boundaries, indicating that defects and impurities are decorated almost entirely on one side of the subgrain boundaries. In addition, the D1 and D2 lines are demonstrated to have different origins due to their significantly varying behaviors after processing steps. D1 is found to be enhanced when the dislocations are cleaned of metal impurities, whereas D2 remains unchanged. Finally, the D4 and D3 lines are proposed to have different origins since their energy levels are shifted differently as a function of distance from the subgrain boundaries.

Index Terms—Crystalline silicon, deep level, dislocations, grain boundaries, photoluminescence (PL), photovoltaic cells.

I. INTRODUCTION

DEEP-LEVEL photoluminescence (PL) spectroscopy has been demonstrated to be a powerful characterization tool for the defects and impurities in photovoltaic silicon [1]. Distinct spectral signatures have been reported for different defects and impurities in crystalline silicon, such as Fe precipitates [2], oxygen precipitates [3], Cr-B pairs [4], and dislocations [5]. In multicrystalline silicon (mc-Si), dislocations are a major limiting factor for the cell efficiency, and often occur at small angles and other subgrain boundaries (sub-GBs) due to high thermal stresses during ingot growth and cooling [6]. Therefore, understanding the deep-level spectra of dislocations is important to improve the material quality and, thus, the final efficiency of mc-Si solar cells.

The so-called D lines, emitted from dislocations, have been studied intensively regarding their thermal behaviors [7]–[10]; spatial distributions [1], [11]–[16]; process-related changes [7]; [17]; and polarization features [1], [7], [18], [19]. The doublet

D1/D2 has been hypothesized to originate from the surrounding local conditions, such as neighboring dislocations or stress by Arguirov *et al.* [8] and Lee *et al.* [15], or from decorating defects and impurities located around dislocations by Sugimoto *et al.* [13]. On the other hand, the doublet D3/D4 was believed to represent the intrinsic nature of dislocations [8], [15]. This was confirmed recently by Tajima *et al.* [1], [20], who employed micro-PL (μ PL) spectroscopy with a high spatial resolution to examine the distribution of D lines around the sub-GBs, finding that D1/D2 were distributed around the sub-GBs, whereas D3/D4 were located directly at the sub-GBs.

However, various authors have reported varying behaviors of the D1 and D2 lines at cryogenic temperatures. Some reported spectra in which the D2 line was a less-significant peak embedded on the high-energy side of the intense D1 line [7], [11], [12], [14]. Others reported spectra with the D2 line present, but with D1 absent [9], [13]. Some pointed out a large change in the D1/D2 intensity ratio depending on the locations in the wafers [8], [21], [22], inconsistent thermal behaviors between D1 and D2 [8], or the difference in mapping images of D1 compared with other D lines [15]. Therefore, some uncertainty remains regarding the connection between D1 and D2.

In addition, although the intensity ratio of the doublet D3/D4 does not vary as strongly as that of D1/D2, there is still an inconsistency among reported works. Near liquid nitrogen temperature, the D4 peak was reported to be higher than the D3 peak in [7] and [11]. However, the opposite observation was presented in other works [8], [23]. Sekiguchi *et al.* [21] found the varying intensity ratio of D3/D4 along the slip lines of dislocations, and suggested that D3 is not the phonon replica of D4. Recently, employing a hyperspectral PL imaging technique at 110 K, Burud *et al.* [22] had the same findings in mc-Si wafers, and proposed that D3 and D4 could have different origins.

In this study, utilizing a μ PL mapping system with spatial resolution of about 3 μ m, along with well-controlled sample preparation steps, we investigate the behaviors and origins of D lines in mc-Si wafers. We first study the micrometer-scale spatial distribution of these D lines around sub-GBs at 79 K, revealing a distinctly asymmetrical distribution for D1/D2. We also compare the behavior of the D lines after different processing steps including phosphorus diffusion gettering, high-temperature annealing, and controlled contamination with Fe. From these results, we clarify some of the uncertainties about the origins and properties of the D lines.

Manuscript received January 6, 2015; revised February 11, 2015; accepted February 19, 2015. Date of publication March 13, 2015; date of current version April 17, 2015. This work was supported by the Australian Research Council and the Australian Renewable Energy Agency under research Grant RND009.

H. T. Nguyen, F. E. Rougieux, and D. Macdonald are with the Research School of Engineering, The Australian National University, Canberra, ACT 2601, Australia (e-mail: hieu.nguyen@anu.edu.au; fiacre.rougieux@anu.edu.au; daniel.macdonald@anu.edu.au).

F. Wang and H. Tan are with the Department of Electronic Materials Engineering, The Australian National University, Canberra, ACT 2601, Australia (e-mail: fan.wang@anu.edu.au; Hoe.Tan@anu.edu.au).

Color versions of one or more of the figures in this paper are available online at <http://ieeexplore.ieee.org>.

Digital Object Identifier 10.1109/JPHOTOV.2015.2407158

II. EXPERIMENTAL DETAILS

The investigated samples are directionally solidified, boron-doped p-type mc-Si wafers with nominal resistivity of $1.6 \Omega\cdot\text{cm}$, corresponding to a background doping of about $9 \times 10^{15} \text{ cm}^{-3}$. We prepared four samples cut from four consecutive sister wafers sliced from the same ingot. These samples were first chemically etched with an etchant consisting of hydrofluoric and nitric acids to remove saw damage and to achieve optically polished surfaces. After that, the first sample was kept in the as-cut state. The second sample went through an extended phosphorous gettering process, in which it was processed at $880 \text{ }^\circ\text{C}$ for 60 min in a mixture of POCl_3 vapor, O_2 , and N_2 , and then was cooled down to $650 \text{ }^\circ\text{C}$ and left there for another 12 h in N_2 gas [24]. The sheet resistance of the resultant diffused layer was around $30 \Omega/\square$. The third sample went through the same thermal processing step as the gettering process but with only N_2 gas, giving the same thermal budget as the second sample but without phosphorous gettering. The fourth sample was gettered in the same way as the second one, and then its diffused layer was etched off. It was then implanted with a low energy (70 keV) Fe dose of $2.4 \times 10^{12} \text{ cm}^{-2}$ and annealed at $900 \text{ }^\circ\text{C}$ for 35 min in O_2 gas to distribute the Fe uniformly across the wafer thickness. After that, this sample was cooled down to $600 \text{ }^\circ\text{C}$ and left for 20 h to allow Fe to precipitate along the GBs and sub-GBs [25]. All samples were chemically etched again to remove all the residual layers (diffused, implanted, and thermal oxide layers) left after the previous processing steps. Finally, they were immersed in a defect etchant consisting of acetic/nitric/hydrofluoric acids for 16 h. The purpose of this etching step is to delineate the sub-GBs, which are, otherwise, not observable under the optical microscope. The optical image of an investigated sub-GB is provided in Fig. 2(d). The investigated sub-GBs were located far away from other sub-GBs to avoid confounding effects from neighboring sub-GBs.

The μPL spectroscopy system employed in this study is a Horiba T64000 equipped with a confocal microscope. A $50\times$ reflective objective lens was used to focus the incident laser beam into a spot of about $1 \mu\text{m}$ in diameter on the samples, and to direct the emitted PL signal into a monochromator as well. This emitted signal was then collected by a liquid-nitrogen-cooled InGaAs array detector. The monochromator gratings were set at 150 grooves/mm for PL, providing a spectral resolution of 0.25 nm. The spectral response of the entire system was calibrated with black body thermal radiation emitted from a black body cavity. The employed laser was a diode-pumped solid-state laser having a wavelength of 532 nm, and an on-sample average intensity of 6 mW. The sample stage was equipped with X and Y positioners with the smallest step size of $0.2 \mu\text{m}$. The line scans across the sub-GBs had a step size of $2 \mu\text{m}$, and those along the sub-GBs had a step size of $5 \mu\text{m}$. The sample temperature was kept constant at 79 K with a liquid-nitrogen cryostat, since the spectral distribution of the D lines is resolved more clearly at these lower temperatures. The radial spatial resolution of the technique was determined by the injection level, the temperature, and the defect density and was estimated to be about $3 \mu\text{m}$ for the intragrain regions, where it is limited by the

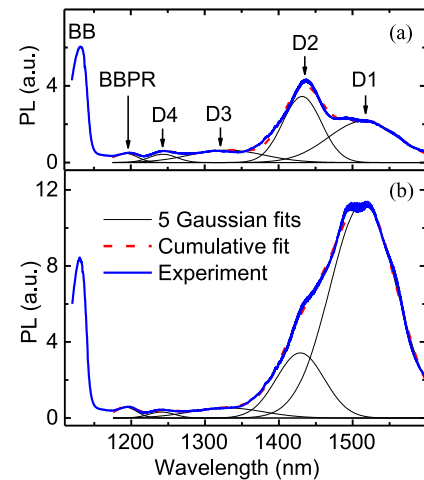


Fig. 1. Comparison of the deep-level PL spectra between the (a) as-cut and (b) gettered samples at a distance of about $20 \mu\text{m}$ from the sub-GB at 79 K.

Auger-dominated diffusion length of excess carriers. This spatial resolution is better near the sub-GBs due to the reduced carrier diffusion lengths via increased Shockley–Read–Hall recombination.

III. RESULTS AND ANALYSIS

Fig. 1(a) and (b) shows our spectra captured at a distance about $20 \mu\text{m}$ from the same sub-GB for the first (as-cut) and second (gettered) samples, respectively. We numerically decomposed the spectra and fitted them with five Gaussian distributions, corresponding to the first phonon replica of the band–band line (BBPR) and the D4, D3, D2, and D1 lines. The peak heights of these Gaussian functions represent the intensity of their corresponding lines. The narrow band–band (BB) line is at around 1130 nm and clearly distinguished from these five lines. Thus, we were able to accurately determine the peak height of the BB line without needing to decompose it from the other lines.

First, we consider the spatial distribution of the D1 and D2 lines around the sub-GB. Fig. 2(a) and (b) plots the amplitudes of D1 and D2 (after the total spectrum is decomposed), along with the BB peak, versus the distance away from the sub-GB for the as-cut and gettered samples, respectively. Each line scan, in fact, consists of two sections, which were started from the same location on the sub-GB and then extended in opposite directions away from the sub-GB. The two spectra measured directly on the sub-GB of the two scanning sections were found to be the same, allowing us to combine the results from these two scanning sections into one line scan. By scanning this way, we can ensure correct positioning of sub-GBs in the center of the scan, and minimize potential impacts of the imperfect alignment of the X and Y positioners on the area around sub-GBs. The distributions of D1 and D2 appear to be very asymmetric across this sub-GB. In order to ensure that this asymmetry is not a measurement artifact, we performed line scans across this sub-GB at another location, which was shifted about $40 \mu\text{m}$ compared with the previous location. Again, in Fig. 2(c) and (d), the asymmetric distributions of D1 and D2 are still present on the same side.

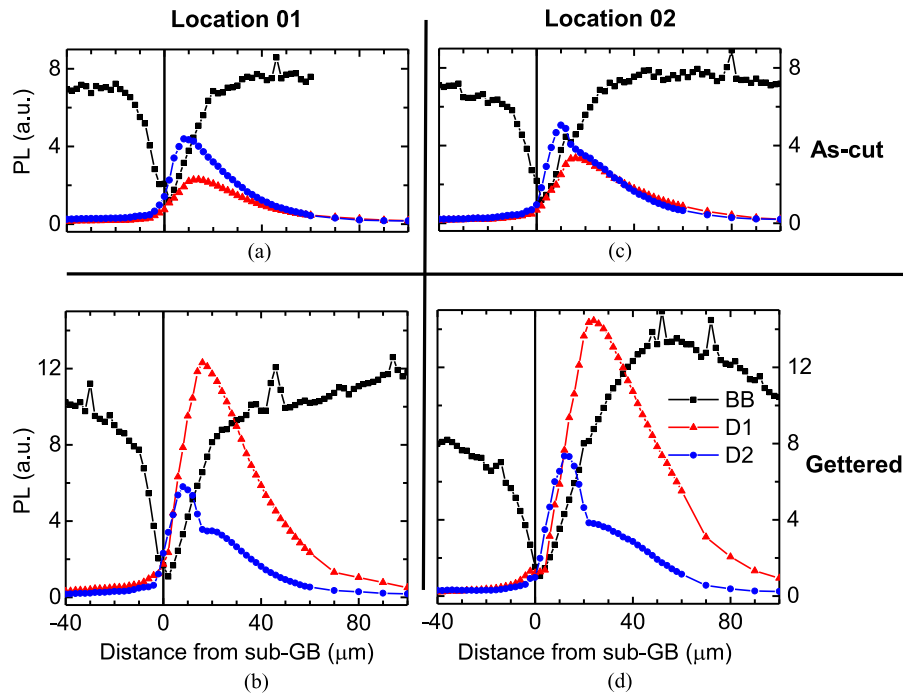


Fig. 2. [(a) and (c)] Line scans across the sub-GB of the intensities of D1, D2, and BB lines at two locations for the as-cut and gettered [(b) and (d)] samples. Location 02 [(c) and (d)] was shifted about $40 \mu\text{m}$ along the same sub-GB compared to location 01 [(a) and (b)]. The vertical line at zero distance indicates the location of the sub-GB.

Note that in Fig. 2, although the BB distribution is also asymmetric, the extent of this asymmetry is much less pronounced than those of D1 and D2 indicating that the observed asymmetry is not due to a difference in local injection levels or other optical artifacts. We found this asymmetry of D1 and D2 at all sub-GBs on the samples investigated in this paper (at approximately ten sub-GBs).

Moreover, right at the sub-GB, the intensities of both D1 and D2 are very low, and then increase when moving away from the sub-GB. This signature is consistent with the hypothesis that D1 and D2 originate from secondary defects or impurities trapped around the dislocations, as suggested by Tajima *et al.* [1], [20]. Thus, the above asymmetry suggests that these secondary defects and impurities are distributed almost entirely on one side of the sub-GBs. This asymmetry has not been observed in previous reports due to their lower spatial resolution, for example, several tens of micrometers in the case of Tajima *et al.* [20]. Note that the step size of our line-scans is only $2 \mu\text{m}$ and, thus, smaller than the estimated $3 \mu\text{m}$ spatial resolution due to carrier diffusion. Therefore, there is likely to be some degree of signal smearing in the line scans. However, the spatial extent of the observed asymmetry extends to several tens of micrometers, and thus, is much larger than the impact of any smearing caused by carrier diffusion.

Since D1 and D2 luminescence centers are originated from defects or impurities trapped by the strain field around the dislocations, the asymmetry of D1 and D2 could be due to the higher local stress on one side of the sub-GB, which was formed during the ingot cooling process. However, such stress usually extends to only a few micrometers from the dislocation sites [26], while the observed asymmetry in this study extends to several tens of

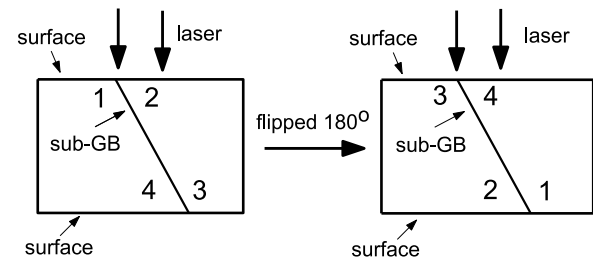


Fig. 3. Inclined sub-GB. If the asymmetry of D1 and D2 is an artifact due to the inclination, the higher intensities of D1 and D2 should be observed at side 2 before flipping and at side 4 after flipping. However, D1 and D2 were observed at side 2 and side 3 and were absent at side 1 and side 4.

micrometers. In addition, we did not observe any shift in the silicon Raman peak when performing Raman scans across this sub-GB indicating that the stress is not significantly different between two sides of this sub-GB [26]. Therefore, the hypothesis of different local stress causing the asymmetry of D1 and D2 is unlikely to be correct.

Another hypothesis is that the observed asymmetry of D1 and D2 may stem from an inclination of this sub-GB compared with the surface. However, again the asymmetry extends to several tens of micrometers, whereas the investigated samples are only about $250\text{-}\mu\text{m}$ thick. Hence, the inclination angle of this sub-GB would need to be unusually large for this hypothesis to be true, considering that the sense depth of the measurements is only several micrometers. In addition, as illustrated in Fig. 3, if the observed asymmetry is an artifact caused by the inclined sub-GB, we should have higher luminescence intensities of D1 and D2 at side 2 before rotating and flipping the sample, and at

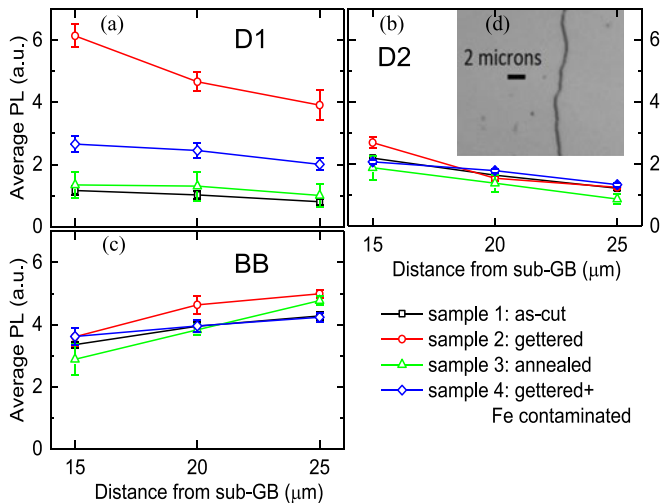


Fig. 4. Comparison of (a) D1, (b) D2, and (c) BB average intensities among the four samples at different distances from the same sub-GB at 79 K, including one standard deviation error bars. (d) Microscope image of this sub-GB.

side 4 afterward. However, we still observed higher intensities of D1 and D2 at side 3 after flipping the sample. Thus, this second hypothesis is also incorrect. Moreover, since the higher intensities of D1 and D2 appear on the opposite side of the sub-GB (relative to the initial scan direction) after flipping the sample, the observed asymmetry is not an artifact caused by the choice of scan direction. We, therefore, propose that the notable asymmetry of D1 and D2 is due to the defects and impurities being preferentially decorated on one side of the sub-GB during the crystal growth process. More microscopic studies are needed to understand the reasons for this preferential decoration.

Furthermore, as readily seen from Figs. 1 and 2, the D1 intensity is enhanced significantly relative to the BB intensity after getting, whereas the D2 peak is not altered significantly. In order to avoid any localized variability of the sub-GB skewing our conclusions, we performed 60- μm long line scans (13 data points per scan) parallel to this sub-GB at different distances away from it on the side of high D1 and D2 intensities. The D1 and D2 average intensities (after decomposing the spectrum) from these line scans are depicted in Fig. 4(a) and (b), respectively, for the four sister samples. D1 again shows a significant enhancement after the extended phosphorous getting process, whereas D2 remains unchanged. Note that the BB signal is also largely unchanged among all the samples, as shown in Fig. 4(c), indicating that the enhancement of D1 after getting is not due to an increased local injection level.

The phosphorus getting process used here has been demonstrated to be very effective in monocrystalline silicon, in which more than 99% of dissolved Fe impurities can be removed [24]. However, our samples are mc-Si. Thus, besides this external getting, the second sample may also experience internal getting, in which at least some metal impurities are preferentially decorated around the GBs and sub-GBs instead of being captured in the phosphorus diffused layers [27]. Therefore, although the global concentration of metal impurities such as Fe will be reduced by the external getting, the local concentration

at GBs and sub-GBs could, in principle, actually be higher than that of the as-cut sample.

We, therefore, performed similar line scans along the same sub-GB at similar distances for the third sample. Since this sample has the same thermal budget as the phosphorous getting process, but without phosphorous getting, it is expected that there would be a greater extent of metal impurities decorated around the sub-GBs due to the internal getting effects. However, from Fig. 4(a), the D1 intensity is the same as the as-cut sample, prompting us to speculate that the enhancement of D1 in the phosphorous gettered sample is due to a reduction of metal impurities near the sub-GBs after the phosphorous getting process. To fortify this hypothesis, we performed the scanning on the fourth sample. The concentration of Fe impurities around the sub-GBs of this gettered and Fe implanted sample should be higher than that of the gettered sample. However, the D1 intensity is significantly lower than that of the gettered sample. Therefore, we conclude that D1 is enhanced when the sub-GBs are cleaned of metal impurities. This behavior may be explained by the fact that D1 and D2 are due to the secondary defects trapped around dislocation sites. When metal impurities are present, they may form complexes with the D1 centers; thus, altering their energy levels and reducing their luminescence efficiency. When the metal impurities are removed by getting, the D1 centers become radiatively active again, and hence, the D1 intensity is increased significantly.

The above finding can be compared with the results from Tajima *et al.* [28], who reported that the D1 line was unchanged, but the D2 line was suppressed after their sample was contaminated with Fe. We also found many sub-GBs in which D1 and D2 were not altered by the getting process, compared with the as-cut sample. Nevertheless, based on the remarkably different behaviors of D1 and D2 in our study, we also conclude that D1 is not the phonon replica of D2 and that they have different origins.

Next, we inspect the behaviors of the D3 and D4 lines. In order to avoid being confounded by the strong tails of D1 and D2, we chose another sub-GB in which D3 and D4 are strong, but D1 and D2 are completely absent. Fig. 5(a) and (b) displays the line scan intensity of D3 and D4 peaks using the Gaussian fitting method as described above. The line scanning was performed at similar locations across the same sub-GB for the first and second samples. From Fig. 5(a) and (b), the D3 and D4 intensities are flattened at the sub-GB. This signature is consistent with the fact that these two lines reflect the intrinsic nature of dislocations [1], [8], [15], [20]. However, we observed slightly asymmetric distributions of D3 and D4 across this sub-GB, although this asymmetry is certainly not as strong as that of D1 and D2. This slight asymmetry may be due to the fact that the dislocation density is slightly different between two sides of the sub-GB. In addition, the intensities of D3 and D4 still remain the same between the as-cut and gettered samples. In other words, D3 and D4 are not affected by the getting process, which is consistent with the hypothesis that D3 and D4 are intrinsic properties of the dislocations themselves.

Furthermore, Fig. 5(c) shows the PL spectra normalized to the BB peak at different distances from the sub-GB of

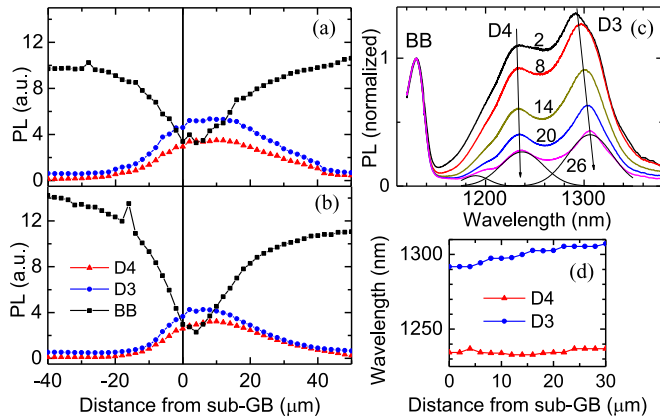


Fig. 5. Line scans of the intensities of D3, D4, and BB lines across a sub-GB of the (a) as-cut and (b) gettered samples at 79 K. The vertical line at zero distance indicates the location of this sub-GB. (c) Spectra of the as-cut sample at different distances in micrometer, indicated by the number on each spectrum, from the sub-GB was normalized to the BB peak. The Gaussian fits of the spectrum at 26 μm are also plotted (thin black lines). (d) Peak wavelengths of D3 and D4 versus the distance from the sub-GB.

the as-cut sample. The energy level of D4 is constant as a function of distance, whereas the D3 peak moves toward higher wavelengths (lower energies) at farther distances. Fig. 5(d) quantitatively shows the energy shifts for both D3 and D4. The energy level was determined by choosing the wavelength at the local maxima of PL intensity around D3 and D4. This observation contradicts the common belief from the literature that D3 is the phonon replica of D4 [8], [20]. If D3 is the transverse-optical phonon replica of D4, their peak energies should be consistently shifted by around 57 meV [29]. However, this energy difference varies from 42 to 54 meV in Fig. 5(d). We note that this finding regarding D3 and D4 could not be easily observed with a spatial resolution of several tens of micrometers or above, as was the case in most previous works in the literature. Thus, we hypothesize that D3 is not the phonon replica of D4 and that they may have different origins.

IV. CONCLUSION

Utilizing high spatial resolution and well-controlled processing steps, we have experimentally demonstrated the asymmetry of D lines across the sub-GBs in mc-Si wafers. In addition, we have shown the different origins of the D1 and D2 lines, and concluded that D1 is suppressed by the presence of metal impurities near the dislocations, although not via quenching caused by a reduction in the excess carrier density. Finally, we have proposed that D3 is not the phonon replica of D4 and that these two lines may have different origins due to their different energy shifts as a function of distance from the sub-GBs.

ACKNOWLEDGMENT

The authors would like to thank R. Elliman for access to the ion implant facility, and K. Belay, S. Surve, C. Samundsett, T. Ratcliff, J. Bullock, and A. Y. Liu for assisting with the sample preparation, as well as The Australian National Fabrication

Facility for providing access to some of the facilities used in this paper.

REFERENCES

- [1] M. Tajima, "Spectroscopy and topography of deep-level luminescence in photovoltaic silicon," *IEEE J. Photovoltaics*, vol. 4, no. 6, pp. 1452–1458, Nov. 2014.
- [2] P. Gundel, M. C. Schubert, W. Kwapił, J. Schön, M. Reiche, H. Savin, M. Yli-Koski, J. A. Sans, G. Martinez-Criado, W. Seifert, W. Warta, and E. R. Weber, "Micro-photoluminescence spectroscopy on metal precipitates in silicon," *Physica Status Solidi, Rapid Res. Lett.*, vol. 3, pp. 230–232, 2009.
- [3] S. Binetti, S. Pizzini, E. Leoni, R. Somaschini, A. Castaldini, and A. Cavallini, "Optical properties of oxygen precipitates and dislocations in silicon," *J. Appl. Phys.*, vol. 92, pp. 2437–2445, 2002.
- [4] H. Conzelmann and J. Weber, "Photoluminescence from chromium-boron pair in silicon," *Physica B+C*, vol. 116, pp. 291–296, 1983.
- [5] R. Sauer, J. Weber, J. Stolz, E. R. Weber, K.-H. Küsters, and H. Alexander, "Dislocation-related photoluminescence in silicon," *Appl. Phys. A*, vol. 36, pp. 1–13, 1985.
- [6] B. Sopori, P. Rupnowski, V. Mehta, V. Budhbraja, S. Johnston, N. Call, H. Mouninho, M. Al-Jassim, A. Shaikh, M. Seacrist, and D. Carlson, "Performance limitations of mc-si solar cells caused by defect clusters," *ECS Trans.*, vol. 18, no. 1, pp. 1049–1058, 2009.
- [7] S. Ostapenko, I. Tarasov, J. P. Kalejs, C. Haessler, and E.-U. Reisner, "Defect monitoring using scanning photoluminescence spectroscopy in multicrystalline silicon wafers," *Semicond. Sci. Technol.*, vol. 15, pp. 840–848, 2000.
- [8] T. Arguirov, W. Seifert, M. Kittler, and J. Reif, "Temperature behaviour of extended defects in solar grade silicon investigated by photoluminescence and EBIC," *Mater. Sci. Eng. B*, vol. 102, pp. 251–256, 2003.
- [9] M. C. Schubert, P. Gundel, M. The, W. Warta, M. Romero, S. Ostapenko, and T. Arguirov, "Spatially resolved luminescence spectroscopy on multicrystalline silicon," in *Proc. 23rd Eur. Photovoltaic Sol. Energy Conf.*, Valencia, Spain, 2008, pp. 17–23.
- [10] F. Dreckschmidt and H.-J. Möller, "Defect luminescence at grain boundaries in multicrystalline silicon," *Phys. Status Solidi C*, vol. 8, pp. 1356–1360, 2011.
- [11] I. Tarasov, S. Ostapenko, W. Seifert, M. Kittler, and J. P. Kalejs, "Defect diagnostics in multicrystalline silicon using scanning techniques," *Physica, Condensed Matter*, vol. 308–310, pp. 1133–1136, 2001.
- [12] M. Kittler, W. Seifert, T. Arguirov, I. Tarasov, and S. Ostapenko, "Room-temperature luminescence and electron-beam-induced current (EBIC) recombination behaviour of crystal defects in multicrystalline silicon," *Sol. Energy Mater. Sol. Cells*, vol. 72, pp. 465–472, 2002.
- [13] H. Sugimoto, M. Inoue, M. Tajima, A. Ogura, and Y. Ohshita, "Analysis of intra-grain defects in multicrystalline silicon wafers by photoluminescence mapping and spectroscopy," *Jpn. J. Appl. Phys.*, vol. 45, pp. L641–L643, 2006.
- [14] M. Inoue, H. Sugimoto, M. Tajima, Y. Ohshita, and A. Ogura, "Microscopic and spectroscopic mapping of dislocation-related photoluminescence in multicrystalline silicon wafers," *J. Mater. Sci. Mater. Electron.*, vol. 19, pp. S132–S134, 2008.
- [15] W. Lee, J. Chen, B. Chen, J. Chang, and T. Sekiguchi, "Cathodoluminescence study of dislocation-related luminescence from small-angle grain boundaries in multicrystalline silicon," *Appl. Phys. Lett.*, vol. 94, pp. 112103-1–112103-3, 2009.
- [16] R. P. Schmid, D. Mankovics, T. Arguirov, M. Ratzke, T. Mchedlidze, and M. Kittler, "Rapid dislocation-related D1-photoluminescence imaging of multicrystalline Si wafers at room temperature," *Physica Status Solidi A*, vol. 208, pp. 888–892, 2011.
- [17] S. Binetti, A. Le Donne, and M. Acciarri, "Processing step-related upgrading of silicon-based solar cells detected by photoluminescence spectroscopy," *Sol. Energy Mater. Sol. Cells*, vol. 86, pp. 11–18, 2005.
- [18] M. P. Peloso, J. S. Lew, P. Chaturvedi, B. Hoex, and A. G. Aberle, "Polarisation analysis of luminescence for the characterisation of defects in silicon wafer solar cells," *Prog. Photovoltaics, Res. Appl.*, vol. 20, pp. 661–669, 2011.
- [19] G. Kato, M. Tajima, H. Toyota, and A. Ogura, "Polarized photoluminescence imaging analysis around small-angle grain boundaries in multicrystalline silicon wafers for solar cells," *Jap. J. Appl. Phys.*, vol. 53, pp. 080303-1–080303-3, 2014.

- [20] M. Tajima, Y. Iwata, F. Okayama, H. Toyota, H. Onodera, and T. Sekiguchi, "Deep-level photoluminescence due to dislocations and oxygen precipitates in multicrystalline Si," *J. Appl. Phys.*, vol. 111, pp. 113523-1-113523-6, 2012.
- [21] T. Sekiguchi and K. Sumino, "Cathodoluminescence study on dislocations in silicon," *J. Appl. Phys.*, vol. 79, pp. 3253-3260, 1996.
- [22] I. Burud, A. S. Flø, and E. Olsen, "On the origin of inter band gap radiative emission in crystalline silicon," *AIP Advances*, vol. 2, pp. 042135-1-042135-7, 2012.
- [23] C. Krause, D. Mankovics, H.-M. Krause, Tz. Arguirov, and M. Kittler, "On the origin of intense luminescence at 0.93 eV from multi-crystalline silicon," *J. Appl. Phys.*, vol. 114, pp. 034902-1-034902-6, 2013.
- [24] S. P. Phang and D. Macdonald, "Direct comparison of boron, phosphorus, and aluminum gettering of iron in crystalline silicon," *J. Appl. Phys.*, vol. 109, pp. 073521-1-073521-6, 2011.
- [25] A. Y. Liu and D. Macdonald, "Precipitation of iron in multicrystalline silicon during annealing," *J. Appl. Phys.*, vol. 115, pp. 114901-1-114901-10, 2014.
- [26] P. Gundel, M. C. Schubert, and W. Warta, "Simultaneous stress and defect luminescence study on silicon," *Physica Status Solidi A*, vol. 207, pp. 436-441, 2010.
- [27] D. Macdonald, A. Y. Liu, and S. P. Phang, "External and internal gettering of interstitial iron in silicon for solar cells," *Solid State Phenom.*, vol. 205, pp. 26-33, 2013.
- [28] M. Tajima, M. Ikebe, Y. Ohshita, and A. Ogura, "Photoluminescence analysis of iron contamination effect in multicrystalline silicon wafers for solar cells," *J. Electron. Mater.*, vol. 39, pp. 747-750, 2010.
- [29] K. L. Shaklee and R. E. Nahory, "Valley-orbit splitting of free excitons? The absorption edge of Si," *Phys. Rev. Lett.*, vol. 24, pp. 942-945, 1970.

Authors' photographs and biographies not available at the time of publication.